Data Management in Structural Health Monitoring

SS#1: Data Management in Structural Health Monitoring

Elia Favarelli, Enrico Testi, and Andrea Giorgetti*

Dept. of Electrical, Electronic, and Information Engineering "Guglielmo Marconi"
University of Bologna, 40136 Bologna, Italy
{elia.favarelli2, enrico.testi4, andrea.giorgetti}@unibo.it

Abstract. With the advent of 5G and the future 6G communication systems, the number of devices interconnected to the network will increase exponentially, offering unprecedented monitoring capability. The autonomous structural health monitoring (SHM) of many structures and bridges represents an important application that can exploit such capability; however, generating a considerable amount of data that must be elaborated and managed. In such a scenario, this paper proposes a set of machine learning (ML) tools to detect anomalies in a bridge from vibrational data. The proposed framework starts from the first two fundamental frequencies extracted through operational modal analysis (OMA) and clustering, followed by a density-based time-domain tracking algorithm. The fundamental frequencies extracted are then fed to one-class classification (OCC) algorithms that perform anomaly detection. Then, the effect of reducing the number of sensors used to monitor the network, the number of bits used to quantize the accelerometric measurements, and the observation time is reported, with the purpose to reduce the amount of data stored without degrading the damage detection capability of the system. As a case study, the *Z-24* bridge is considered because of the extensive database of accelerometric measurements in both standard and damaged conditions. In numerical results a widely comparison of OCC algorithms is reported; more in detail, principal component analysis (PCA), kernel principal component analysis (KPCA), Gaussian mixture model (GMM) and one-class classifier neural network (OCCNN)^2 are tested and their robustness is evaluated. In many cases, OCCNN^2 algorithm increases the performance with respect to classical anomaly detection techniques in terms of accuracy. Moreover, it is observed that only three sensors are sufficient to accomplish the anomaly detection task and that the number of bits and the observation time can be reduced considerably without affecting the algorithms' performance.

Keywords: Anomaly detection · dimensionality reduction · modal analysis · neural network · structural health monitoring · vibration measurement.

* E. Favarelli 0000-0001-9266-4880, E. Testi 0000-0003-2238-9160, and A. Giorgetti 0000-0001-6341-3927.

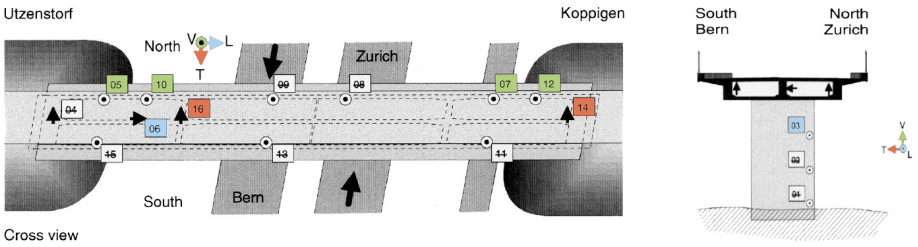

Fig. 1. Data acquisition setup along the *Z-24* bridge: the selected accelerometers, their positions, and the measured acceleration direction [13].

1 Introduction

Nowadays, structural health monitoring (SHM) represents a fundamental research field in a society where historical and modern infrastructures coexist harmoniously. In this scenario, despite replacing the existing infrastructures, buildings, and bridges with functionally and economically costly solutions, it is preferred to maintain and protect the existing structures [1]. This preservation can be achieved through appropriate monitoring.

As far as bridges are concerned, some statistics highlight the relevance of the problem. For example, currently, in Italy there are almost 2000 bridges that require special monitoring; in France, 4000 bridges need to be restored, and 840 are considered in critical conditions; in Germany, 800 bridges are reputed critic; in the United States of America, among the 600.000 bridges, according to a conservative estimate, at least 1% of them is considered deficient. In this sense, SHM offers numerous solutions for anomaly detection [2–4].

In literature, numerous damage detection and localization strategies have been presented and tested [5, 6]. Part of them focuses on the extraction of the most significant damage-sensitive features of the structure under analysis. Such techniques can be divided into model-free and model-based: in the former, information is gathered by measurements (e.g., acceleration, temperature, position), while in the latter, data comes from measurements and prior knowledge of a model of the structure [7].

Since the whole procedure results complex and requires a specific fine-tuning of several parameters that depend on the structure under analysis, the adoption of machine learning (ML) techniques to detect changes in the damage sensitive features received increasing interest recently [8–12].

In this work, we attempt to investigate strategies to detect anomalies in bridges and structures with a reduced number of sensors, samples, and resolution bits, to find low-cost solutions and reducing the data storage requirements, with the aim to extend this strategy to an extensive set of infrastructures. The proposed framework starts from the fundamental frequencies extraction from the accelerometer measurements through stochastic subspace identification (SSI), cleaning, and clustering [7, 8, 14–18] and then performs modal frequencies track-

ing in the time domain [11]. The first two fundamental frequencies are then considered as a feature space used to train one-class classifiers to perform damage detection. In particular, the main contributions are the following:

- We compare several ML algorithms performance for the anomaly detection task.
- We propose strategies to reduce the amount of data stored to detect anomalies in structures.
- We investigate the effect of sensor failure on algorithm performance.
- We evaluate the effects of reducing the number of samples on the classification accuracy.
- We consider the effect of resolution bits to account for low-cost sensors unavoidable in large-scale monitoring.

The performance of the proposed solution is investigated on a real dataset using the accelerometric data available for the *Z-24* bridge [19,20]. The proposed anomaly detection algorithms principal component analysis (PCA), kernel principal component analysis (KPCA), Gaussian mixture model (GMM), and one-class classifier neural network (OCCNN)^2 are compared in terms of accuracy.

Throughout the paper, capital boldface letters denote matrices and tensors, lowercase bold letters denote vectors, $(\cdot)^{\mathrm{T}}$ stands for transposition, $||\cdot||$ is the ℓ_2-norm of a vector, and $\mathbb{1}\{a, b\}$ is the indicator function equal to 1 when $a = b$, and zero otherwise.

The paper is organized as follows. In Section 2, a brief overview of the acquisition system, the accelerometers setup, and the monitoring scenario is presented. The fundamental frequencies extraction technique adopted is rapidly revised in Section 3. A survey of anomaly detection techniques is reported in Section 4. The traffic generated by the acquisition system and some possible strategies to reduce it are presented in Section 5. Numerical results are given in Section 6. Conclusions are drawn in Section 7.

2 System Configuration

The *Z-24* bridge was located in the Switzerland canton Bern. The bridge was a part of the road connection between Koppigen and Utzenstorf, overpassing the A1 highway between Bern and Zurich. It was a classical post-tensioned concrete two-cell box girder bridge with a main span of 30 m and two side spans of 14 m. The bridge was built as a freestanding frame with the approaches backfilled later. Both abutments consisted of triple concrete columns connected with concrete hinges to the girder. Both intermediate supports were concrete piers clamped into the girder. An extension of the bridge girder at the approaches provided a sliding slab. All supports were rotated with respect to the longitudinal axis that yielded a skew bridge. The bridge was demolished at the end of 1998 [19]. During the year before its demolition, the bridge was subjected to long-term continuous monitoring to quantify the bridge dynamics' environmental variability. Moreover, progressive damage tests took place over a month, shortly before the complete

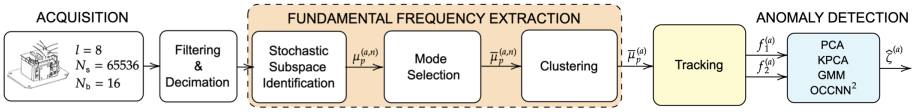

Fig. 2. Block diagram for signal acquisition, processing, feature extraction, tracking, and anomaly detection.

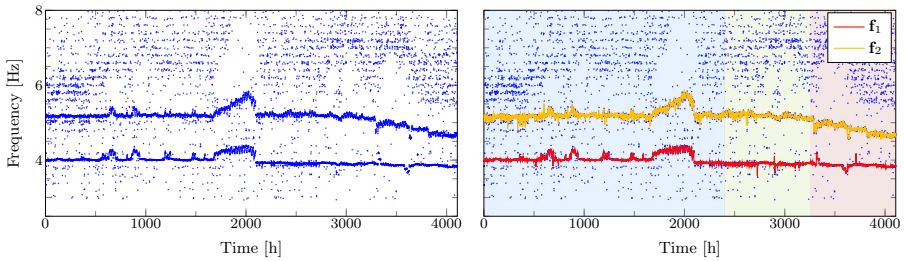

Fig. 3. On the left, fundamental frequencies extracted through SSI for each measurement on the right first two natural frequencies estimation after the density-based tracking algorithm. Blue and green backgrounds highlight the acquisitions made during the bridge's normal condition, used respectively as training and test sets, while the red background stands for damaged condition acquisitions used in the test phase.

demolition of the bridge, alternated with short-term monitoring tests while the continuous monitoring system was still running. The tests proved experimentally that realistic damage has a measurable influence on bridge dynamics.

2.1 Data collection

The accelerometer's position and their measurement axis are shown in Fig. 1. In this work, we considered $l = 8$ accelerometers, identified as 03, 05, 06, 07, 10, 12, 14, and 16, which are present in both long-term continuous monitoring phase and in the progressive damage one.[1] The accelerometer orientation is highlighted in Fig. 1 with different colors, red, green, and blue, staying respectively for transversal, vertical, and longitudinal orientation. Every hour $N_\mathrm{s} = 65536$ samples are acquired from each sensor with sampling frequency $f_\mathrm{samp} = 100\,\mathrm{Hz}$ which corresponds to an acquisition time $T_\mathrm{a} = 655.36\,\mathrm{s}$. Since the measurements are not always available, there are $N_\mathrm{a} = 4107$ acquisitions collected in a period of 44 weeks.

[1] Some accelerometers that experienced failures during the long-term monitoring have been avoided.

2.2 Data pre-processing

The block diagram depicted in Fig. 2 represents the sequence of tasks performed for the fully automatic anomaly detection approach presented in this work.

Some pre-processing steps have been applied to the data to reduce disturbs, the computational cost, and the memory occupation of the subsequent elaborations. First, a decimation by a factor of 2 is applied to each acquisition; hence the sampling frequency is scaled to $f_{\text{samp}} = 50\,\text{Hz}$. Such sampling frequency is considered sufficient because the *Z-24* fundamental frequencies fall in the [2.5, 20] Hz frequency range [19]. After decimation, data are processed with a finite impulse response (FIR) band-pass filter of order 30 with band [2.5, 20] Hz, to remove disturbances outside the band of interest.

At the end of the decimation step, the amount of samples for each acquisition N_{dec} is already halved ($N_{\text{dec}} = N_{\text{s}}/2 = 32768$) and that represent a first important step in the data management process.

3 Frequency Extraction and Data Partitioning

The fundamental frequencies extraction chain is depicted in Fig. 2; from the vibrational data the fundamental modes $\mu_p^{(a,n)}$ are extracted through the widely known SSI algorithm [7], where p represent the pth mode, a stays for the acquisition index, and n represent the model order varied in the range $n \in [2, 160]$ (with step 2) [11]. The resulting modes can be cleaned up by the spurious ones though classical mode selection methods (i.e., modal assurance criterion (MAC), mean phase deviation (MPD), complex conjugate poles check, and damping ratios check) [15,17,18,21] and clustered with the K-means algorithm [8,14]. The residual modes after selection are represented with $\bar{\mu}_p^{(a,n)}$, and the modes after clustering with $\bar{\mu}_p^{(a)}$. The results of this approach applied for all the acquisitions are the blue points depicted in Fig. 3. After that, a density-based mode tracking algorithm is proposed to track the fundamental frequencies; firstly the algorithm is initialized evaluating 200 acquisition to detect the number of tracks s and their starting position, after that trough a Gaussian kernel evaluation their position is update step-by-step for each acquisition [11]. At the end of the tracking algorithm the first two fundamental frequency tracks $\mathbf{f}_s = \left\{ f_s^{(a)} \right\}_{a=1}^{N_{\text{a}}}$ with $s \in \{1, 2\}$ are extracted and stored in the following matrix (see also Fig. 3b)

$$\mathbf{F} = \begin{bmatrix} \mathbf{f}_1 \\ \mathbf{f}_2 \end{bmatrix}^{\text{T}} = \begin{bmatrix} f_1^{(1)} & f_1^{(2)} & \dots & f_1^{(N_{\text{a}})} \\ f_2^{(1)} & f_2^{(2)} & \dots & f_2^{(N_{\text{a}})} \end{bmatrix}^{\text{T}}.$$

At this point, the fundamental frequencies extracted must be divided into training, test in standard condition, and test in damaged conditions sets. As described in [19], the damage is introduced at the acquisition $a = N_{\text{d}} = 3253$, corresponding to the installation of a lowering system. Therefore, from now on, the matrix $\bar{\mathbf{X}} = \mathbf{F}_{1:2N_{\text{d}}-N_{\text{a}}-1,:}$ contains the training points (blue background in Fig. 3b),

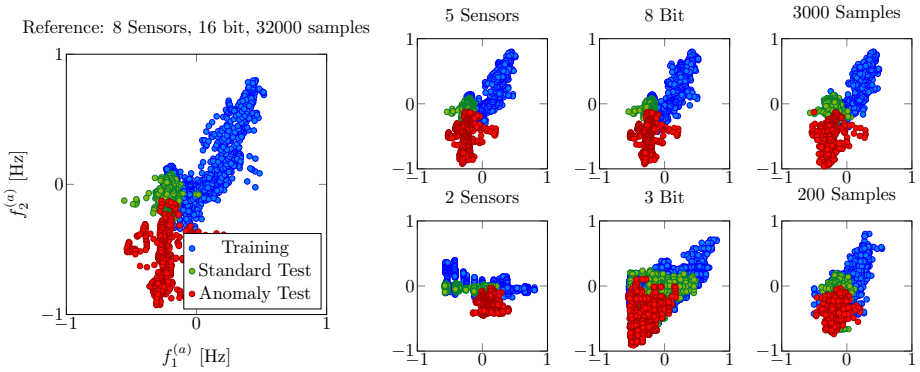

Fig. 4. Examples of feature transformation due to the effect of a low number of sensors, a low number of bits, and a low number of samples with respect to the standard measurement condition reported on the left.

$\bar{\mathbf{Y}} = \mathbf{F}_{2N_\mathrm{d}-N_\mathrm{a}:N_\mathrm{d}-1,:}$ contains the test points in standard condition (green background in Fig. 3b), and $\bar{\mathbf{U}} = \mathbf{F}_{N_\mathrm{d}:N_\mathrm{a},:}$ contains the test points in damaged condition (red background in Fig. 3b). The three subsets of acquisitions that correspond to training, standard test, and damaged test points are, respectively, $\mathcal{I}_\mathrm{x} = \{1, ..., 2N_\mathrm{d} - N_\mathrm{a} - 1\}$, $\mathcal{I}_\mathrm{y} = \{2N_\mathrm{d} - N_\mathrm{a}, ..., N_\mathrm{d} - 1\}$, and $\mathcal{I}_\mathrm{u} = \{N_\mathrm{d}, ..., N_\mathrm{a}\}$.

Let us define the offset $\hat{\mathbf{x}}$ as the column vector containing the row-wise mean of the matrix $\bar{\mathbf{X}}$, and the rescaling factor $x_\mathrm{m} = \max_{a,s} |\bar{x}_{a,s} - \hat{x}_a|$. Before proceeding with the anomaly detection, the matrices $\bar{\mathbf{X}}$, $\bar{\mathbf{Y}}$ and $\bar{\mathbf{U}}$ are centered and normalized subtracting the offset $\hat{\mathbf{x}}$ row-wise and dividing each entry by the rescaling factor x_m. The resulting data matrices are $\mathbf{X}$, $\mathbf{Y}$ and $\mathbf{U}$, of size $N_\mathrm{x} \times D$, $N_\mathrm{y} \times D$, and $N_\mathrm{u} \times D$, respectively, with $D = 2$ features. The result of this procedure is depicted on the left of Fig. 4.

4 Survey of Anomaly Detection Techniques

In this section we briefly review PCA, KPCA, GMM which are often adopted for one-class classification (OCC) and introduce OCCNN^2, a neural network based approach recently presented [22–26].

4.1 Principal component analysis

This technique remaps the training data from the feature space $\mathbb{R}^D$ in a subspace $\mathbb{R}^P$ (where $P < D$ is the number of components selected) that minimizes the Euclidean distance between the data in the feature space and their projection into the chosen subspace [27]. To find the best subspace to project the training data, the evaluation of the $D \times D$ sample covariance matrix

$$\boldsymbol{\Sigma}_\mathrm{x} = \frac{\mathbf{X}^\mathrm{T}\mathbf{X}}{N_\mathrm{x} - 1} \tag{1}$$

is needed. The sample covariance matrix $\boldsymbol{\Sigma}_{\mathrm{x}}$ can be factorized by eigenvalue decomposition as $\boldsymbol{\Sigma}_{\mathrm{x}} = \mathbf{V}_{\mathrm{x}}\boldsymbol{\Lambda}_{\mathrm{x}}{\mathbf{V}_{\mathrm{x}}}^{\mathrm{T}}$, where $\mathbf{V}_{\mathrm{x}}$ is an orthonormal matrix whose columns are the eigenvectors, while $\boldsymbol{\Lambda}_{\mathrm{x}}$ is a diagonal matrix that contains the D eigenvalues. The eigenvalues magnitude represents the importance of the direction pointed by the relative eigenvector. In our setting we select the largest component, hence $P = 1$, therefore the best linear subspace of dimension one is $\mathbf{v}_{\mathrm{P}}$, which coincides with the eigenvector related to the largest eigenvalue of $\boldsymbol{\Sigma}_{\mathrm{x}}$. The projection into the subspace is obtained multiplying the data by $\mathbf{v}_{\mathrm{P}}$, i.e., $\mathbf{x}_{\mathrm{P}} = \mathbf{X}\mathbf{v}_{\mathrm{P}}$, $\mathbf{y}_{\mathrm{P}} = \mathbf{Y}\mathbf{v}_{\mathrm{P}}$, and $\mathbf{u}_{\mathrm{P}} = \mathbf{U}\mathbf{v}_{\mathrm{P}}$.

The error is evaluated reconstructing the data in the original feature space, i.e., $\widetilde{\mathbf{X}} = \mathbf{x}_{\mathrm{P}}\mathbf{v}_{\mathrm{P}}^{\mathrm{T}}$, $\widetilde{\mathbf{Y}} = \mathbf{y}_{\mathrm{P}}\mathbf{v}_{\mathrm{P}}^{\mathrm{T}}$, and $\widetilde{\mathbf{U}} = \mathbf{u}_{\mathrm{P}}\mathbf{v}_{\mathrm{P}}^{\mathrm{T}}$. After the reconstruction, it is possible to calculate the error as the Euclidean distance between the original and reconstructed data.

Unfortunately, PCA is usually ineffective whit a low number of monitored modes; moreover, the variability of the frequencies estimated due to environmental effects can affect the PCA performance [28]. This is because PCA can find only linear boundaries in the original feature space; hence it is recommended when the problem dimensionality of the problem is high and the boundaries between the classes can be considered linear.

4.2 Kernel principal component analysis

Due to the inability of PCA of finding non-linear boundaries, here we propose KPCA as an alternative [29]. KPCA firstly maps the data with a non-linear function, named kernel, then applies the standard PCA to find a linear boundary in the new feature space. The kernel function, applied to the linear boundary, makes it non-linear in the original feature space. A delicate point in the development of KPCA algorithm is the kernel function choice. In [30], where the data distribution is unknown, the radial basis function (RBF) kernel is proposed as the right candidate. Given a generic point $\mathbf{z}$ that correspond to a $1 \times D$ vector, we can apply the RBF as

$$K_n^{(\mathbf{z})} = e^{-\gamma||\mathbf{z}-\mathbf{x}_n||^2}, \quad \text{with} \quad n = 1, 2, \ldots, N_{\mathrm{x}} \tag{2}$$

where γ is a kernel parameter (which controls the width of the Gaussian function) that must be set properly, $\mathbf{x}_n$ is the nth row of $\mathbf{X}$, and $K_n^{(\mathbf{z})}$ is the nth component of the point $\mathbf{z}$ in the kernel space. Overall, the vector $\mathbf{z}$ is mapped in the vector $\mathbf{k}^{(\mathbf{z})} = [K_1^{(\mathbf{z})}, K_2^{(\mathbf{z})}, \ldots, K_{N_{\mathrm{x}}}^{(\mathbf{z})}]$. Remapping all the data in the kernel space, we obtain the subsequent matrices $\mathbf{K}_{\mathrm{x}}$ of size $N_{\mathrm{x}} \times N_{\mathrm{x}}$ for training, $\mathbf{K}_{\mathrm{y}}$ of size $N_{\mathrm{y}} \times N_{\mathrm{x}}$ for validation, and $\mathbf{K}_{\mathrm{u}}$ of size $N_{\mathrm{u}} \times N_{\mathrm{x}}$ for test, respectively.

Applying now the PCA to the new dataset, it is possible to find non-linear boundaries in the original feature space.

4.3 Gaussian mixture model

Another well-known data analysis tool, named GMM, has been used to solve OCC problems in literature [31]. This approach assumes that data can be rep-

resented by a mixture of $\mathcal{M}$ multivariate Gaussian distributions. The outputs of the algorithm are the covariance matrices, $\boldsymbol{\Sigma}_m$, and the mean values, $\boldsymbol{\mu}_m$, of the Gaussian functions, with $m = 1, 2, \ldots, \mathcal{M}$. The GMM algorithm finds the set of parameters $\boldsymbol{\Sigma}_m$ and $\boldsymbol{\mu}_m$ of a Gaussian mixture that better fit the data distribution through iterative algorithms like stochastic gradient descent or Newton-Raphson [8, 9].

4.4 One-Class Classifier Neural Network^2

This algorithm exploits the flexibility of the standard feed-forward neural network (NN) in an anomaly detection problem. It is based on the OCCNN paradigm [24] that provide to generate artificially anomalous points with a spatial density proportional to the one inferred by the Pollard's estimator [32]. Such anomalous points will be used during the training to estimate the class boundaries. This procedure is repeated several times to refine the edges step-by-step. Unfortunately, Pollard's estimator may exhibit accuracy degradation when the dataset points distribution deviates from Poisson. Based on these considerations, the OCCNN^2 share the same strategy of OCCNN but the first boundary estimation is made by an autoassociative neural network (ANN) that provide good boundaries estimation also with non-Poisson data distributions [11].

5 Data Management

This section analyzes the amount of data that must be stored to perform anomaly detection on the vibrational waveforms and some strategies that can be implemented to reduce such volume of data. Considering a network of $l = 8$ synchronized sensors interconnected to a coordinator that stores the accelerometric measurements, it is easy to observe that if each sensor collects $N_\mathrm{s} = 65536$ samples each acquisition with $N_\mathrm{b} = 16$ resolution bits, the total amount of data stored by the coordinator is $M_\mathrm{t} = N_\mathrm{s} N_\mathrm{b} N_\mathrm{a} l \simeq 32\,\mathrm{Gbit} = 4\,\mathrm{GB}$ for $N_\mathrm{a} = 4107$ acquisitions. This considerable amount of data has been stored in an year of non continuous measurements, where the actual acquisition time is $T_\mathrm{t} = T_\mathrm{a} N_\mathrm{a} \simeq 44860\,\mathrm{m} \simeq 448\,\mathrm{h}$. The volume of data in a continuous measurement system in a year would be around 47 GB. To reduce the mass of data the first step is decimation. Considering that in this application the fundamental frequencies of the bridge fall in the interval $[0, 20]\,\mathrm{Hz}$, to comply with the sampling theorem with a guard band of 5 Hz a sampling frequency $f_\mathrm{samp} = 50\,\mathrm{Hz}$ is enough to capture the bridge oscillations. Since the measurements are acquired by accelerometers with $f_\mathrm{samp} = 100\,\mathrm{Hz}$, a decimation by factor 2 can be adopted so that data volume is halved: $M_\mathrm{d} = M_\mathrm{t}/2 \simeq 2\,\mathrm{GB}$. Starting from the decimated waveforms, three other tunable parameters can be modified to reduce the volume of data without deteriorating the performance of the OCC algorithms significantly:

- The number of sensors l; this also reduces the network costs.

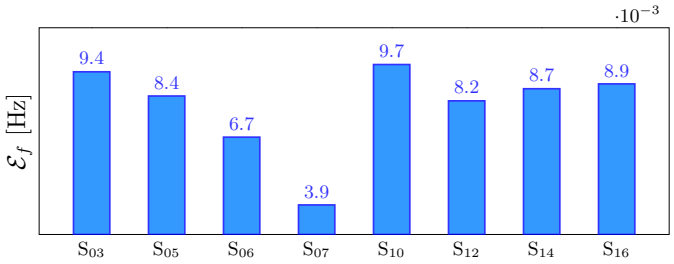

Fig. 5. Error produced removing the selected sensor.

- The number of samples N_s or equivalently the acquisition time T_a; this has benefits also on the energy consumption and network lifetime in battery-powered sensors [33, 34].
- The number of bits N_b; this also reduces the accelerometer cost.

All these possibilities will be analyzed and widely discussed in the next section. In Fig. 4 some working points of the system are reported and compared with the reference working condition after decimation ($l = 8$, $N_\mathrm{d} = 32768$, $N_\mathrm{b} = 16$).

6 Numerical Results

In this section, the proposed algorithms are applied to the *Z-24* bridge dataset to detect anomaly based on the fundamental frequencies estimation [7, 35, 36], and a reduced number of features. The performance is evaluated through the accuracy, considering only the test set:

$$\text{Accuracy} = \frac{T_\mathrm{P} + T_\mathrm{N}}{T_\mathrm{P} + T_\mathrm{N} + F_\mathrm{P} + F_\mathrm{N}} \tag{3}$$

where T_P, T_N, F_P, and F_N, represent respectively true positive, true negative, false positive, and false negative predictions. Such indicators are obtained comparing the actual labels $[\zeta^{(1)}, \ldots, \zeta^{(N_\mathrm{a})}]$, with those predicted by the OCC $[\widehat{\zeta}^{(1)}, \ldots, \widehat{\zeta}^{(N_\mathrm{a})}]$. In this application, labels are 0 for normal condition and 1 for anomaly condition, respectively. Therefore,

$$T_\mathrm{P} = \sum_{a \in \mathcal{I}_\mathrm{u}} \mathbb{1}\left\{\zeta^{(a)}, \widehat{\zeta}^{(a)}\right\} \quad \text{and} \quad T_\mathrm{N} = \sum_{a \in \mathcal{I}_\mathrm{y}} \mathbb{1}\left\{\zeta^{(a)}, \widehat{\zeta}^{(a)}\right\}$$

with $F_\mathrm{N} = N_\mathrm{u} - T_\mathrm{N}$, and $F_\mathrm{P} = N_\mathrm{y} - T_\mathrm{P}$. In the case of unbalanced classes in the test set, the F_1 (function 1) score represents a more reliable metric to evaluate the performance regarding accuracy: it is the harmonic mean of precision and recall; a perfect model has an F_1 score equal to 1.

The feature space has dimension $D = 2$, and the three dataset used for training, test in normal condition, and damaged condition, have cardinality

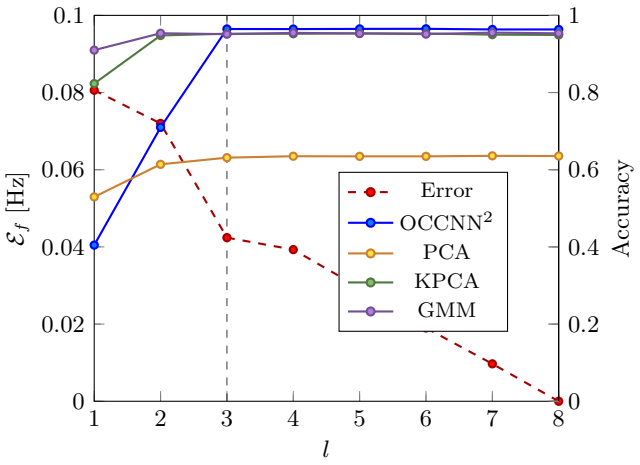

Fig. 6. Error varying the number of sensors available.

$N_\mathrm{x} = 2399$, $N_\mathrm{y} = 854$, and $N_\mathrm{u} = 854$, respectively. For PCA, the number of components selected is $P = 1$. For KPCA, after several tests the values of P and γ that ensure the minimum reconstruction error are $P = 3$ and $\gamma = 8$. For GMM the order of the model that maximize performance is $\mathcal{M} = 10$. Regarding the OCCNN^2 the first step boundary estimation is made by a fully connected ANN with 7 layers of, respectively, 50, 20, 10, 1, 10, 20 and 50 neurons, with ReLU activation functions, and a fully connected NN with 2 hidden layers with $L = 50$ neurons each one for the second step. All the NNs are trained for a number of epochs $N_\mathrm{e} = 5000$ with a learning rate $\rho = 0.05$. The error adopted to evaluate the points displacement in the feature space from the original position due to the different configurations is the root mean square error (RMSE), defined as

$$\mathcal{E}_f = \frac{1}{\sqrt{N_\mathrm{a} N_\mathrm{s}}} \sqrt{\sum_{s=1}^{N_\mathrm{s}} \sum_{n=1}^{N_\mathrm{a}} (f_s^{(n)} - \bar{f}_s^{(n)})^2} \tag{4}$$

where N_s is the number of features ($N_\mathrm{s} = 2$), $f_s^{(n)}$ is the sth feature of the nth acquisition in the initial configuration, and $\bar{f}_s^{(n)}$ is the relative data point in the modified configuration.

6.1 Sensors Relevance

Before evaluating the effect of reducing the number of sensors, it is informative to evaluate each one's importance in the modal frequencies estimation. It is widely known in the literature that the sensor position strongly affects the mode estimation [7]. To verify the sensors' relevance, we removed sensors one-by-one and evaluated the error resulting in the feature space points with respect to

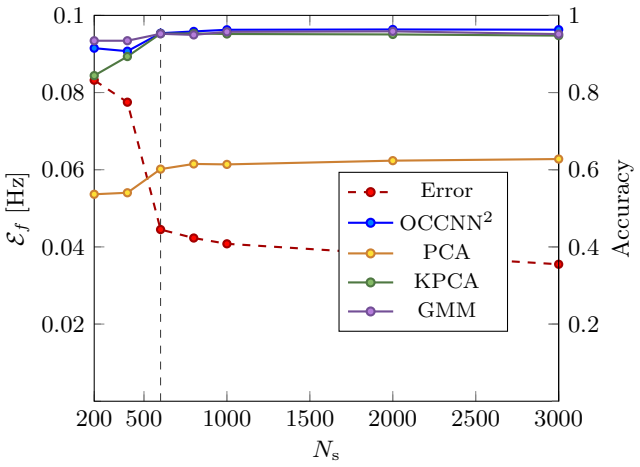

Fig. 7. Error varying the number of samples.

the standard condition. The error is calculated as the RMSE defined previously. As can be seen in Fig. 5, sensor S_{10} generates the most significant error in the fundamental frequencies extraction when removed. With this technique it is possible to sort the sensors from the most relevant to the less one as follows: S_{10}, S_{03}, S_{16}, S_{14}, S_{05}, S_{12}, S_{06}, S_{07}. To evaluate the performance with respect to the number of sensors used to extract fundamental frequencies, the sensors will be removed in the same order, to consider always the worst condition with the given number of sensors.

6.2 Number of Sensors

Now that the sensor relevance is defined, we are able to verify the performance by varying the number of sensors used on the structure to derive the fundamental frequencies with low error. As we can see in Fig. 6 the accuracy of the algorithms remains almost the same as long as the number of sensors available is greater than 2, as the error present a significant increase in correspondence of the gap between 2 and 3 sensors. Thus we can deduce that the minimum number of sensors that must be used to monitor the *Z-24* bridge is equal to 3. In this configuration it is easy to notice that the amount of data stored is reduced to $M_{\text{sen}} = N_{\text{s}} N_{\text{b}} N_{\text{a}} 3 \simeq 0.8\,\text{GB}$.

6.3 Number of Samples

To evaluate the effect of the acquisition time on the anomaly detection performance, we progressively reduced the number of samples used to extract the structure's fundamental frequencies. As we can see in Fig. 7 the performance of the algorithms remain almost constant as long as the number of samples N_{s} is

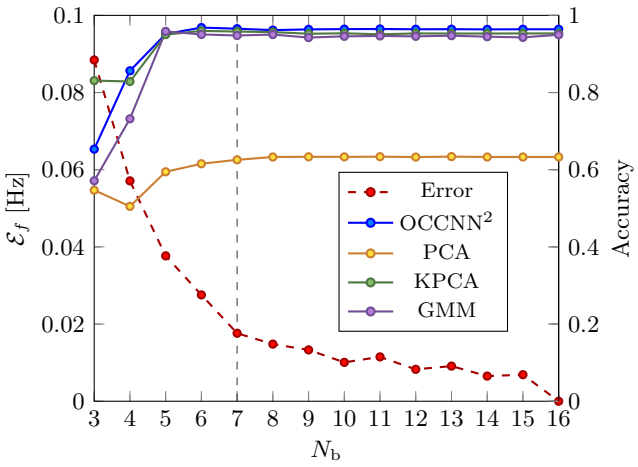

Fig. 8. Error varying the number of bits.

greater than 600, that corresponds to an acquisition time of 12 s with a sampling frequency $f_{\text{samp}} = 50$ Hz. Reducing drastically the acquisition time, we achieve a significant reduction of the data occupation, that in this configuration is $M_{\text{sam}} = 600 N_{\text{b}} N_{\text{a}} l \simeq 0.04$ GB, without performance degradation.

6.4 Number of Bits

he number of bits can also be dropped to reduce the volume of data stored and the accelerometer cost. To test their impact on the performance, we progressively reduced the number of bits used to encode the waveforms extracted from the accelerometers as reported in Fig. 8. As we can see, the error remains contained as far as the number of bits used to encode the samples is greater than 6; likewise, the accuracy of the algorithms remain high as long as the error remains contained. Several low-cost accelerometers are available on the market with a resolution $N_{\text{b}} = 8$, and these results show that this type of sensor could accomplish the anomaly detection task. In this case, the data occupation is $M_{\text{bit}} = 8 N_{\text{s}} N_{\text{a}} l \simeq 1$ GB. This relevant reduction of the number of resolution bits is possible because of the anomaly detector capability to cope with the error introduced in the modal frequencies estimation (depicted in red in Fig. 8) caused by quantization.

7 Conclusion

In this paper, we presented a SHM system that aims to extract damage-sensitive features with the minimum amount of resources necessary for anomaly detection with high accuracy. An overview of some widely used anomaly detection algorithms is provided. Three different approaches are proposed to reduce the

volume of data stored and limit sensors and network infrastructure costs. When the goal is to reduce the amount of data stored, it is good practice to reduce the observation time and use several high-resolution sensors; when the target is to minimize the sensor cost, a good practice is to adopt several low-resolution sensors combined with long observation time; when the objective is to contain the network infrastructure cost, few high-resolution sensors and long observation time can be considered. To evaluate the error introduced by these strategies and the performance of the algorithms, the RMSE and the accuracy are used as metrics, respectively. The results show that these strategies, when properly designed, can be adopted without significant loss of performance; in fact, all the algorithms except the PCA, ensure an accuracy greater than 94% in all of the proposed configurations, with the maximum performance reached by OCCNN^2 whose accuracy never goes down below 95%.

References

1. R. Ferrari, D. Froio, E. Chatzi, F. Pioldi, and E. Rizzi, "Experimental and numerical investigations for the structural characterization of a historic RC arch bridge," in *Proc. Int. Conf. on Comp. Methods in Structural Dynamics and Earthquake Eng.*, vol. 1, Athens, Greece, May 2015, pp. 2337–2353.
2. A. Benedetti, M. Tarozzi, G. Pignagnoli, and C. Martinelli, "Dynamic investigation and short-monitoring of an historic multi-span masonry arch bridge," in *Proc. Int. Conf. on Arch Bridges*, vol. 11, Porto, Portugal, Oct. 2019, pp. 831–839.
3. A. Benedetti, G. Pignagnoli, and M. Tarozzi, "Damage identification of cracked reinforced concrete beams through frequency shift," *Materials and Structures*, vol. 51, pp. 1–15, Oct. 2018.
4. A. Benedetti, C. Colla, G. Pignagnoli, and M. Tarozzi, "Static and dynamic investigation of the Taro masonry bridge in Parma, italy," in *Proc. Int. Conf. on Struct. Analysis of Hist. Const.*, vol. 18, Cusco, Perù, Sep. 2019, pp. 2264–2272.
5. G. D. Roeck, "The state-of-the-art of damage detection by vibration monitoring: the SIMCES experience," *J. of Structural Control*, vol. 10, no. 2, pp. 127–134, May 2003.
6. K. Worden, C. Farrar, J. Haywood, and M. Todd, "A review of nonlinear dynamics applications to structural health monitoring," *Structural Control and Health Monitoring*, vol. 15, no. 4, pp. 540–567, Jul. 2008.
7. G. Fabbrocino and C. Rainieri, *Operational modal analysis of civil engineering structures*. New York: Springer-verlag, May 2014.
8. C. M. Bishop, *Pattern Recognition and Machine Learning*. Springer Verlag, Aug. 2006.
9. J. Watt, R. Borhani, and A. K. Katsaggelos, *Machine Learning Refined*. Cambridge University Press, 2016.
10. I. Goodfellow, Y. Bengio, and A. Courville, *Deep Learning*. MIT Press, 2016.
11. E. Favarelli and A. Giorgetti, "Machine learning for automatic processing of modal analysis in damage detection of bridges," *IEEE Trans. on Instrum. and Meas.*, vol. 70, pp. 1–13, Jan. 2021.
12. L. Pucci, E. Testi, E. Favarelli, and A. Giorgetti, "Human activities classification using biaxial seismic sensors," *IEEE Sensors Letters*, vol. 4, no. 10, pp. 1 – 4, Oct. 2020.

13. Z-24 bridge data. [Online]. Available: https://bwk.kuleuven.be/bwm/z24
14. E. P. Carden and J. M. W. Brownjohn, "Fuzzy clustering of stability diagrams for vibration-based structural health monitoring," *Computer-Aided Civil and Infrastructure Eng.*, vol. 23, no. 5, pp. 360–372, May 2008.
15. C. Wu, H. Liu, X. Qin, and J. Wang, "Stabilization diagrams to distinguish physical modes and spurious modes for structural parameter identification," *Journal of Vibroeng.*, vol. 19, no. 4, pp. 2777–2794, Jun. 2017.
16. C. Rainieri and G. Fabbrocino, "Development and validation of an automated operational modal analysis algorithm for vibration-based monitoring and tensile load estimation," *Mechanical Systems and Signal Processing*, vol. 60-61, pp. 512–534, 2015.
17. A. Cabboi, F. Magalhães, C. Gentile, and Á. Cunha, "Automated modal identification and tracking: Application to an iron arch bridge," *Structural Control and Health Monitoring*, vol. 24, no. 1, p. e1854, Feb. 2017.
18. M. Pastor, M. Binda, and T. Harčarik, "Modal assurance criterion," *Procedia Engineering*, vol. 48, pp. 543–548, 2012.
19. E. Reynders and G. D. Roeck, "Continuous vibration monitoring and progressive damage testing on the z 24 bridge," *Encyclopedia of structural health monitoring*, vol. 10, pp. 127–134, May 2009.
20. E. Reynders, J. Houbrechts, and G. D. Roeck", "Fully automated (operational) modal analysis," *Mechanical Systems and Signal Processing*, vol. 29, pp. 228–250, May 2012.
21. D. Brigante, C. Rainieri, and G. Fabbrocino, "The role of the modal assurance criterion in the interpretation and validation of models for seismic analysis of architectural complexes," in *Proc. Int. Conf. on Structural Dynamics (Eurodin)*, vol. 199, Rome, Italy, Sep. 2017, pp. 3404–3409.
22. A. Santos, M. Silva, C. Sales, J. Costa, and E. Figueiredo, "Applicability of linear and nonlinear principal component analysis for damage detection," in *Proc. IEEE Int. Instr. and Meas. Tech. Conf. (I2MTC)*, Pisa, Italy, May 2015, pp. 869–874.
23. E. Favarelli, E. Testi, L. Pucci, and A. Giorgetti, "Anomaly detection using wifi signal of opportunity," in *Proc. IEEE Int. Conf. on Signal Proc. and Comm. Sys. (ICSPCS)*, Surfers Paradise, Gold Coast, Australia, Dec. 2019, pp. 1–7.
24. E. Favarelli, E. Testi, and A. Giorgetti, "One class classifier neural network for anomaly detection in low dimensional feature spaces," in *Proc. IEEE Int. Conf. on Signal Proc. and Comm. Sys. (ICSPCS)*, Surfers Paradise, Gold Coast, Australia, Dec. 2019, pp. 1–7.
25. P. Perera and V. M. Patel, "Learning deep features for one-class classification," *IEEE Trans. Image Process*, vol. 28, no. 11, pp. 5450–5463, Nov. 2019.
26. R. Chalapathy, A. K. Menon, and S. Chawla, "Anomaly detection using one-class neural networks," *CoRR*, vol. abs/1802.06360, Aug. 2018.
27. H. Abdi and L. J. Williams, "Principal component analysis," *Wiley Interd. Reviews: Comp. Stat.*, vol. 2, no. 4, pp. 433–459, 2010.
28. C. Rainieri, F. Magalhaes, D. Gargaro, G. Fabbrocino, and A. Cunha, "Predicting the variability of natural frequencies and its causes by second-order blind identification," *Structural Health Monitoring*, vol. 18, no. 2, pp. 486–507, 2019.
29. B. Schölkopf, A. Smola, and K.-R. Müller, "Kernel principal component analysis," in *Proc. Int. conf. on artificial neural networks*, vol. 1327, no. 6. Lausanne, Switzerland: Springer, Oct. 1997, pp. 583–588.
30. B. Schölkopf, A. Smola, E. Smola, and K.-R. Müller, "Nonlinear component analysis as a kernel eigenvalue problem," *Neural Comp.*, vol. 10, pp. 1299–1319, Jul. 1998.

31. A. Santos, E. Figueiredo, M. Silva, R. Santos, C. Sales, and J. C. W. A. Costa, "Genetic-based EM algorithm to improve the robustness of gaussian mixture models for damage detection in bridges," *Structural Control and Health Monitoring*, vol. 24, no. 3, p. e1886, May 2017.
32. J. H. Pollard, "On distance estimators of density in randomly distributed forests," *Biometrics*, vol. 27, no. 4, pp. 991–1002, Dec. 1971.
33. M. Chiani and A. Elzanaty, "On the LoRa modulation for IoT: Waveform properties and spectral analysis," *IEEE Internet of Things J.*, pp. 1–8, May 2019.
34. A. Elzanaty, A. Giorgetti, and M. Chiani, "Lossy compression of noisy sparse sources based on syndrome encoding," *IEEE Trans. on Comm.*, vol. 67, no. 10, pp. 7073–7087, Oct. 2019.
35. M. Silva, A. Santos, E. Figueiredo, R. Santos, C. Sales, and J. Costa, "A novel unsupervised approach based on a genetic algorithm for structural damage detection in bridges," *Eng. Applications of Artificial Intelligence*, vol. 52, pp. 168–180, Jun. 2016.
36. M. Silva, A. Santos, R. Santos, E. Figueiredo, C. Sales, and J. C. Costa, "Agglomerative concentric hypersphere clustering applied to structural damage detection," *Mechanical Systems and Signal Processing*, vol. 92, pp. 196–212, Feb. 2017.